5 Laser Materials Processing in Manufacturing of Lithium-Ion Batteries:

Peter Smyrek, Wilhelm Pfleging

Institute for Applied Materials – Applied Materials Physics, Karlsruhe Institute of Technology

P.O. Box 3640, 76021 Karlsruhe, Germany

Abstract

A significant increase in lithium-ion battery performances such as battery lifetime, high-rate capability and fast charging can be achieved by ultrafast laser structuring of composite electrodes. Therefore, laser materials processing and its upscaling in battery manufacturing is currently attracting huge attention as there is an increasing demand to further improve the electrochemical performance of next-generation batteries for use in electric vehicles. However, in addition to laser process upscaling issues, there is a strong need to be able to define suitable three-dimensional (3D) electrode designs regarding application scenarios, respective degradation processes, and safety aspects. Therefore, the development of next generation anodes and cathodes architectures needs to be flanked by analytics capable to generate a rapid evaluation of the entire composite electrodes. An appropriate *post mortem* analytical method should be able to visualize 3D lithium concentration and distribution providing a map of state-of-charge of entire electrodes. Such a technology recently introduced into battery analytics is laser-induced breakdown spectroscopy (LIBS) which is a type of atomic emission spectroscopy providing lateral resolved elemental compositions within a few milliseconds. By combining those chemical data with data from electrochemical analyses an evaluation of thick-film electrode architectures becomes

possible. 2D and 3D lithium concentration profiles are presented for unstructured and laser-structured electrodes and corresponding electrode design criteria are derived from them.

5.1 Introduction

Lithium-ion batteries (LIBs) were first commercially offered by Sony in 1991 [1]. Since then, the demand for maximum power and energy efficiency has increased rapidly. LIBs have become the dominating energy storage technology for electric vehicles (hybrid electric vehicles, plug-in hybrid electric vehicles or fully electric vehicles) as well as for stationary electrochemical storage systems [2]. LIBs are characterized by their relatively high gravimetric energy and power density of 150 Wh/kg to 260 Wh/kg and 340 W/kg to 500 W/kg, respectively. For LIBs, the cost per kilowatt hour was USD 764 in 2009 and could be reduced to USD 111 by 2020 [3-5]. However, it should be noted that the current costs and performance limits of current LIBs still are bottlenecks for electric vehicles and an efficient operation in combination with solar and wind power plants. Efficient stationary storage devices are required to compensate the intermittent properties of e.g., wind turbines, and to smooth their current peaks during power grid feeding.

In the field of lithium-ion battery (LIB) technology current research is concerned with increasing energy and power density by simultaneously lowering production and material costs. Inspired by the commercial success of lithium nickel manganese cobalt oxide ($Li(Ni_{1/3}Mn_{1/3}Co_{1/3})O_2$, NMC 111), new nickel-enriched layered oxides with various compositions ($Li(Ni_{1-x-y}Mn_xCo_y)O_2$, with 1-x-y > 0.5) are currently under intense investigation for increasing the reversible capacity in a lithium-ion cell. Contemporaneously, the manufacturing of electrodes with film thicknesses of about 320 μm could be realized on laboratory scale. Here, the aim is to apply a reduced amount of inactive material and thus, to realize an enhancement of energy density at cell level. As calculated in [6] for NMC 111

batteries (vs. graphite), increasing the layer thickness from state-of-the-art 50 µm to values about 200 µm to 300 µm can contribute to an increase in energy density of more than 20% to 30% up to values of 250 Wh/kg and 580 Wh/L. However, for high-current application the use of thick-film electrodes with thicknesses ≥ 100 µm is conditionally realizable. On the one hand, the mechanical integrity of the electrode layer is impaired, on the other hand, due to high mass loading and areal capacity of > 20 mg/cm^2 and > 4.0 mAh/cm^2, a diffusion overpotential is established, which reduces the available capacity in a lithium-ion cell at a certain C-rate. The term "C-Rate" is used to describe the applied power densities during battery operation. The C-rate indicates the current at which the battery is being discharged and/or charged, based on the practical capacity of the cell. For example, if the C-rate value is C/2 or 2C, the battery will be fully charged or discharged within 2 hours or 30 minutes, respectively.

An effective approach, which enables a battery operation with a simultaneous high energy and power density is based on the so-called "3D-Battery-Concept", which was introduced by J. Long et al. [7] for micro-scaled batteries. Figure 5.1 presents a principle scheme of classical 2D and advanced 3D battery concept [8]. In comparison to the planar electrode arrangement, which represents the current state of the art design (Figure 5.1 a), the electrode geometry is arranged in a three-dimensional (3D) configuration (Figure 5.1 b). According to Long et al. [7], the general strategy of this approach is to fabricate a 3D electrode design including free standing architectures that can maximize power and energy density while maintaining short lithium-ion transportation pathways. An increased active surface area is achieved, which shortens the transport pathways for lithium-ions in liquid electrolyte. It is worth mentioning that the active surface area is referred as the electrode area, which stands in direct contact with the liquid electrolyte. Furthermore, the charge transfer resistance

decreases and a reduction in material stress is expected due to volumetric expansion and contraction during lithiation and delithiation. Finally, the cycle life can be increased [6]. The approach of the 3D-Battery-Concept was mainly motivated for applications in micro- and nano-electromechanical systems [9]. Typically, process technologies such as photolithography, etching processes or thin-film deposition were therefore introduced for the production of 3D micro-batteries [10,11].

Figure 5.1 ABOUT HERE

For classical composite electrodes, as they are nowadays manufactured and integrated in lithium-ion cells, the implementation of the 3D battery concept was demonstrated for the first time by the research group of Pfleging et al. [12-17] at the Karlsruhe Institute of Technology (KIT, IAM-AWP). 3D electrode architectures were generated by laser-assisted processes to improve cycle stability, increase cell lifetime, and realize an accelerated electrolyte filling process. The latter one can be referred to the laser structuring part of the electrode which finally leads to a spontaneous and homogeneous liquid electrolyte wetting [9,18,19]. W. Pfleging et al. [6,20-28] proved that the laser structuring process fulfils the goals of the 3D battery concept. Furthermore, the 3D battery concept can be transferred to different types of cathode materials (e.g. $LiFePO_4$, NMC 111, NMC 532, NMC 622, and NMC 811) with film thicknesses in the range from 50 μm to 250 μm. Pröll et al. [18] were able to show that the wettability of NMC 111 thick-film cathodes was significantly improved by adjusting the 3D battery concept. Due to the generated micro-capillary structures, spontaneous and homogenous wetting with liquid electrolyte was initiated. As a consequence, electrochemical data show that, compared to cells with unstructured electrodes, the operational lifetime increased significantly and an improved cycle stability at elevated C-rates were achieved. Rakebrandt et al. [25] and Zhu et al. [27] demonstrated for

the first time that the process of laser structuring can also be transferred to ultra-thick film NMC electrodes with thicknesses of up to 250 μm. Depending on the electrode film thickness and applied 3D structure, an active mass loss of less than four percent could be achieved. Recently Pfleging`s research group introduced laser-assisted structuring of thick-film electrodes, which are based on self-made water-based production route on cathode and anode side using NMC 622 and silicon-graphite composites, respectively [29-31]. Based on the mentioned pioneering work, several research groups are now heading for the process of laser structuring of battery materials [40-48]. Besides overcoming overpotential problems, one central goal hereby is to counteract fast charging issues of high energy cells by applying the 3D battery concept. Review articles from Pfleging [6,22] and very recently from Li et al. [32] give quite a comprehensive overview about current international approaches in laser processing of battery materials.

In general, the current and future requirements and parameters for next-generation LIBs are shown in Figure 5.2, extracted from [33,34]. In addition to a gravimetric energy density of greater than 275 Wh/kg (at cell level), it is predicted that the cell-level power density will reach values of larger than 800 W/kg. In addition, the charging process should be able to be carried out within 10 to 15 minutes and the total operational lifetime at battery level for fully electric vehicles should be around 2000 cycles [33].

Figure 5.2 ABOUT HERE

Regarding the optimization of electrodes by laser structuring, it is essential to correlate the generated 3D architectures with electrochemical and chemical data. Depending on the electrochemical cycling, conclusions can be drawn about the degradation behaviour of the composite materials. The assessment largely depends on the used characterization method. While *in situ* measurements enable direct monitoring of micro- and nano-scaled processes,

ex situ techniques are effective when higher resolution is required during material characterization [35]. Characterization methods such as energy-dispersive X-ray spectroscopy (EDX), X-ray photoelectron spectroscopy, Auger electron spectroscopy or time-of-flight secondary ion mass spectrometry, offer high lateral resolution. However, they are less effective for volume analyses. Although EDX has a depth resolution in the range of a few microns, it cannot be used as an analysis method for detecting very light elements such as lithium due to the beryllium window.

Laser-induced breakdown spectroscopy (LIBS) is a chemical analysis method that can be used to analyse electrode materials with a depth resolution of about 2 μm to 8 μm. As an application of atomic emission spectroscopy, the elemental composition can be determined either qualitatively or quantitatively within a few milliseconds. Depending on the depth of field of the laser radiation, it is also possible to analyse film thicknesses of up to 500 μm without an adjustment of laser focus position. With the selection of suitable measurement parameters, electrode thick layers can be completely recorded and examined in the range from a few microns up to pouch cell dimensions. LIBS has already been used successfully applied in the field of LIBs material characterization, for example for solid electrolytes [50]. In addition, the binder distribution within the electrode could be qualitatively analysed and described based on the chemical composition (also at interfaces) [6,36,37]. Other publications describe the use of LIBS on thick-film electrodes (anodes and cathodes) to investigate the lithium concentration distribution semi-quantitatively [38-40]. Recent publications show that LIBS is used for parameter optimization of laser-structured NMC 532 cathodes. Depending on the structure geometry and depth, the lithium concentration and its distribution was investigated as a function of the applied C-rate [41]. The use of the LIBS method opens up new possibilities to fully characterize battery materials *post mortem* in

order to be able to draw conclusions about the effects of the electrode design and degradation processes and their origin.

5.2 Materials and Methods

In this chapter, concepts for ultrafast laser-assisted structuring of electrode materials are presented with suitable process sequences. Furthermore, the manufacturing process of thick-film NMC electrodes will be shortly described. Finally, the basic LIBS components for analysing thick film electrodes will be introduced.

5.2.1 Laser materials processing of battery materials

Laser materials processing systems, PS450-TO (Optec s.a., Frameries, Belgium) and MSV-203 (M-Solv Ltd., Oxford, UK), were equipped with different ultrafast laser sources providing medium laser average powers up to 35 W (Satsuma and Tangerine type, Amplitude Systèmes s.a., Bordeaux, France) and ultrafast laser systems with high average laser power of 300 W and 500 W (FX600 types, EdgeWave GmbH, Würselen, Germany). Both processing systems are each equipped with roll-to-roll systems and large field scanner systems to be able to process commercial and advanced electrode materials with a large footprint. The femtosecond lasers operate at a fundamental wavelength of 1030 nm or at its second harmonic (wavelength: 515 nm) with a pulse duration in the range of 280 fs (fs=10^{-15} s) to 10 ps (ps=10^{-12} s). Laser pulse repetition rates from 100 kHz up to 50 MHz can be applied for electrode cutting and structuring [42].

As an example, the PS450-TO laser system equipped with ultrafast fibre laser of type Tangerine will now be described in more detail. The ultrafast fibre laser emits laser radiation in the near infrared range with a fundamental wavelength of 1030 nm and enables pulse lengths in the range from 350 fs to 10 ps. The laser beam is operated in the basic TEM_{00} mode and is specified with a diffraction index of $M^2 < 1.3$. The repetition rate f of the laser

can be variably adjusted in the range from 1 Hz to 2 MHz. A maximum pulse energy of 175 µJ and a maximum average power of P=35 W can be applied. The optical beam path of the PS450-TO laser system is shown schematically in Figure 5.3 a.

Figure 5.3 ABOUT HERE

Starting from the ultrashort pulsed (USP) laser beam source, the laser radiation with a wavelength of 1030 nm is first guided into a frequency converter via a partially transparent deflection mirror. The laser wavelength can then be halved or divided into three (515 nm or 343 nm). Depending on the process application or the degree of absorption of the material, the appropriate selection of the wavelength for laser-assisted processing of materials is crucial. A small part of the laser radiation is guided into an autocorrelator (PulsCheck, APE Angewandte Physik & Elektronik GmbH, Germany) via deflection mirrors. This is used to measure the laser pulse duration which can be adjusted in a range from 350 fs to 10 ps. For the laser radiation emerging from the frequency converter, a wavelength-specific deflection mirror was then used for transmission to a telescope. The electrodes were processed in a process chamber (Figure 5.3 b) using a scanner system (RhothorTM Laser Deflection System, Newson Engineering BV, USA), which has a deflection unit (Rhothor Active Smart Deflector, RTA) with a positioning accuracy of less than 8 µrad and a repeatability of less than 8 µrad. With integrated turret optics, it is also possible to carry out the laser-assisted structuring process with wavelengths in the NIR, VIS and UV ranges without having to move the sample material. Depending on the used optics (F-Theta lens), the focus position on the sample surface is set via an axis that can be moved in the z-direction (accuracy: 0.5 µm, repeatability: ± 1 µm). This is determined using a microscope system, which has an optical zoom and is also attached to the turret optics. In addition to the scanner system, a motorized X and Y positioning table (Aerotech, Inc.) can be used, which is specified with a

positioning accuracy of $\pm$ 1 μm and a repeatability of $\pm$ 0.5 μm. One suitable set of process parameters for laser structuring of NMC 111 electrodes is achieved for a wavelength of 515 nm, a pulse duration of 380 fs and a repetition rate of 500 kHz. The composite layer is removed using the scanning method and using an F-Theta lens with a focal length of 100 mm. Depending on the layer thickness and the degree of porosity of the electrodes, the number of scan repetitions can be varied. Figure 5.4 shows examples of laser-structured electrodes with hole pattern and line pattern for cathode and anode, respectively.

Figure 5.4 ABOUT HERE

5.2.2 Battery materials for cell fabrication

Commercially active materials were selected for electrode coating development via tape casting with a doctor blade (ZUA 2000.100, Proceq, Schwerzenbach, Switzerland) using a lab coater (MSK-AFA-L800-LD, MTI Corporation, Richmond, CA, USA). The thickness of the electrode composite layers was controlled by varying the gap of the doctor blade. On cathode side NMC powders such as NMC 111 powder (MTI Corporation, USA), NMC 622 (BASF SE, Ludwigshafen, Germany), and NMC 811 (ECOPro BM, Chungcheongbuk-do, Korea) were used while on anode side active materials were applied such as flake-like graphite (Targray, Technology International Inc., Kirkland, QC, Canada) and/or nano-sized silicon particles (2W iTech, LLC, San Diego, CA, USA). For slurry preparation different types of binders were introduced such as NMP-based polyvinylidene fluoride (PVDF, MTI corporation, USA), water-based carboxymethyl cellulose (CMC, CRT 2000PA, DoeWolff Cellulosic, Bomlitz, Germany), styrene-butadiene rubber (SBR) (MTI Corporation, USA), and water-based fluorine acrylic copolymer latex TRD 202A (JSR Micro NV, Leuven, Belgium). Finally, carbon black C-NERGY Super C65 (Imerys G & C Belgium,Willebroek, Belgium) or Timcal Super C65 (MTI Corporation, Richmond, CA, USA) were used as

conductive additives. Detailed descriptions of the respective recipes for anodes and cathodes can be found in [30,43,44] and [31,45,46], respectively. The slurries were tape casted onto thin metallic aluminium (cathode) and copper (anode) current collector foils. Prior to laser structuring, the electrode was calendered using a hot rolling press machine (HR01 Hot Rolling Machine, MTI Corporation, Richmond, CA, USA). Finally, the manufactured electrodes reveal a porosity of 35 % (cathode) and 42 % (anode).

As an example for used electrode materials, Figure 5.5 a shows a photograph of the wet film after the tape casting process has been carried out. The wet film was dried at 90°C. The subsequent characterization of the produced electrodes was initially carried out by SEM investigations (Figure 5.5 b, c). The NMC secondary particles, which are surrounded by binder (PVDF) and conductive carbon black (Timcal Super C65) are composed of individually irregular primary particles.

<div align="center">Figure 5.5 ABOUT HERE</div>

In a further processing step, the manufactured NMC thick film cathodes were calendered. The calendering process is essential in the production of lithium-ion batteries. On the one hand, it is ensured that the particle density increases during the compression and, on the other hand, an improvement in the adhesion of the layer on the current conductor is guaranteed. Care must be taken to make sure that the desired porosity of the electrodes is adjusted.

5.2.3 Laser induced breakdown spectroscopy (LIBS)

Laser-induced breakdown spectroscopy (LIBS) was used to determine lithium concentration profiles in thick-film electrodes. A passively mode-locked diode-pumped neodymium-doped yttrium-aluminium-garnet solid-state laser (Nd:YAG) with a fundamental wavelength of nm was used to generate the plasma. The repetition rate can be variably adjusted in a range from

1 Hz to 100 Hz. The pulse energy and pulse duration are 3 mJ and 1.5 ns, respectively. The laser beam was guided via an optical fibre and subsequently focused onto the electrode surface using a focusing mirror with a focal length of 75 mm. The radiation emission of the plasma was then coupled in an optical fibre bundle and fed into two spectrometers arranged in parallel (type: AvaSpec-ULS2048XL, Avantes, Netherlands). The detector covers spectral ranges of 229 – 498 nm and 569 – 792 nm. The data were analysed by SEC Viewer 1.9 (Secopta GmbH, Teltow, Germany). The measured intensity of the elements detected in the plasma was visualized as a function of the emission wavelength [47]. The identified were assigned with the help of the NIST database [48]. Due to the sensitivity of the LIBS method for light elements such as lithium, the two Li^I peaks at λ=610.4 nm and λ=670.8 nm are particularly pronounced. However, the Li^I peak at 670.8 nm was excluded from the calibration due to the observed self-absorption effect [49]. Further intense peaks, which can be assigned to the transition metals Ni, Mn, and Co in the excited state, can be also detected [47]. The oxygen contained in the NMC cathode was detected in the wavelength range from 777.2 nm to 777.5 nm but was neglected for the later LIBS calibration. The reason for this is that the LIBS measurements were carried out in ambient air and this can lead to values in the oxygen determination that are subject to uncertainty. No data was recorded in the wavelength range from 499.7 nm to 568.2 nm because this range was not covered by the used detectors.

The measurement position on the sample surface was set with an axis system (X-direction) and with a positioning table that can be moved in the Y-direction. An additional camera attached to the axis system (Z-direction) was used to adjust the focus position. In addition, the visual recognition system was used to determine the impact position of the first laser pulse with high accuracy (±5 μm) via an "offset" relative to the laser beam focusing optics.

For a typical measurement area of 13 mm x 13 mm, a total number of 17,161 spectra per layer were recorded. Due to the effect of self-absorption at the wavelength of 670.8 nm, the Li^I emission wavelength of 610.4 nm was used for the analysis of lithium [47]. The calibration data were derived from LIBS and inductively coupled plasma optical emission spectroscopy (ICP-OES) as described in [47,50]. Lithium concentration and distribution related to C-rates were systematically investigated in structured and unstructured electrodes [30,43,47,50-52].

5.3 Lithium concentration profiles in unstructured NMC thick film electrodes

The use of electrodes with high mass loading is currently one of the most promising strategies to increase the volumetric/gravimetric energy density of the lithium-ion battery while using the well-established types of active materials. In production of such high-energy electrodes, approaches are presented with the aim to reduce inactive cell components (e.g., current collector, separator) [6,53]. It could be shown in case of a 52 Ah battery (NMC 111 vs. graphite) that by increasing of the cathode film thickness from 50 µm up to 125 µm and 250 µm the specific energy density at cell level can be increased by 18 % and 27 %, respectively [6]. However, a further increase in layer thickness shows a saturation effect for the enhancement of volumetric and gravimetric energy density at the cell level. Taking into account that roll-to-roll processing of electrode material should be still possible, it can be assumed that the maximum electrode film thicknesses in the range of 200 µm to 300 µm (for each side of the current collector) might be technical feasible.

Regarding low C-rates ($< C/2$), the thick film approach might be still practicable. However, with the use of higher C-rates ($> C/2$) for cells with ultra-thick film electrodes, the electrochemical performance of the cell is severely impaired [54]. For example, Lee et al. [55] achieved less than 20% of the practical capacity at a C-rate of 2C for cathodes with a

mass loading of about 25 mg/cm^2. Another aspect that poses challenges for the use of high-mass loaded electrodes is the wetting of electrodes with liquid electrolyte. The filling process becomes more complex and time consuming as the layer thickness increases, especially in the case of electrode configurations with low porosity [6,18,22]. In case of insufficient electrode wetting with liquid electrolyte dry areas with electrochemical inactivity are formed, especially in the deeper layers of the electrode which are close to the current collector. Those areas provide preferred starting points for degradation processes such as lithium plating. From LIBS analysis data, a model scheme description for NMC thick-film cathodes could be set up, which illustrates the possible degradation processes and respective locations within the cell. In a study published by Park et al. [56] NMC standard and high-energy electrodes were produced with an active mass loading of 20 mg/cm^2 and 28 mg/cm^2 which correspond to layer thicknesses of 70 μm and 100 μm, respectively. Depth profile measurements were carried out using LIBS in order to determine qualitatively the lithium distribution of NMC thick electrodes after manufacturing. The depth resolution which corresponds to the material removal per laser pulse during the LIBS measurement was in the range of 7 μm to 10 μm. The relative lithium concentration was normalized to the intensity of the first measurement, each time recorded on the surface of the NMC thick film electrode. The procedure was repeated for each data set of the depth profiles. The area of electrode exposed to the LIBS measurements was not specified. It becomes clear that the values of the lithium content for electrodes after manufacturing vary as a function of the electrode depth - starting from the electrode surface. For the standard electrode, the relative lithium content varies in the range from 0.95 to 1.125. The minimum value being detected after the second laser pulse. The maximum value of the lithium content is assigned to the seventh pulse, which corresponds to an electrode depth of 49 μm. The LIBS analysis on the high-mass

loaded electrode also shows no significant change and deviation in the lithium concentration. The variation in the lithium content is almost in the same range, with a minimum and maximum of the lithium content after the fifth and tenth laser pulse, respectively. For the electrodes manufactured in [50], the averaged lithium concentration after the coating process was in the range of 0.99 ± 0.01 and 1.09 ± 0.02, which indicates a uniform particle distribution in the measured electrode. The relative lithium concentration does not provide any information about quantitative data that could indicate, for example, over-lithiation of the cathode material. However, the study shows that LIBS as an analysis method in the field of battery development enables the detection of lithium concentration profiles. To investigate the lithium content in electrochemically cycled electrodes, Park et al. [56] assembled half cells (vs. Li/Li^+) in coin cell design. The galvanostatic measurements were carried out using the constant-current (CC) method, with the LIBS analysis being carried out *post mortem* after cycle number 25th, 50th, 75th, and 100th.

The strong influence of the number of cycles, which significantly influences the lithium distribution both on the electrode surface and in the deeper regions of the electrode, could be shown. The inhomogeneous lithium distribution is clearly pronounced from a number of cycles of 50, in which the electrodes show an increase or decrease in lithium concentration in regions close to the current collector, depending on the process (charging or discharging). According to Park et al. [56] the relative lithium concentration nearby the current collector at the end of the charging cycle is significantly higher than on the electrode surface. It can be assumed that the charging process in the electrode near the interface between the composite material and the current collector was not completed. The increased lithium concentration is confirmed with an increase in the number of cycles and in particular after a number of cycles in the range between 75 and 100. In the discharged state, the electrode also shows an

inhomogeneous distribution of the lithium content. However, compared to the charged state, the level of non-uniformity appears to be much less pronounced. Park et al. [56] explained this behaviour with the fact that the discharging process begins with a charged state, which already contains a lower lithium content in the region close to the electrode surface. Furthermore, it was pointed out that during discharging the top layer achieves a much faster recovery of the lithium content, which indicates the significant inhomogeneity of the reaction in the electrode. The LIBS results obtained by Smyrek et al. [50] could confirm the results of Park et al. [56] in a first approximation and for selected positions in the electrode. Those results will be presented in the chapter.

5.4 LIBS for evaluation of degradation processes in unstructured NMC thick film electrodes

To investigate the influence of cell cycling regarding the lithium concentration and its distribution in the composite material, unstructured NMC 111 thick-film electrodes were assembled into half-cells. *Post mortem* LIBS was applied in order to determine the lithium concentration on the sample surface and in the entire electrode. In a first approach, the electrodes were measured after the formation process. For the NMC 111 cathode, the voltage range was set from 3.0 V to 4.2 V. The proportion of lithium-ions extracted from the cathode material was in the range of 50% to 55%, so that the practical specific capacity corresponds to a value of around 150 mAh/g. The formation was performed with a C-rate of C/10 (charging and discharging) for a total of three cycles. The cell was then disassembled, the cathode material was washed in DMC and subsequently characterized by using LIBS. In general, it can be observed that the lithium concentration shows a homogeneous distribution after the formation process of the lithium-ion cell [50].

To evaluate the lithium concentration distribution in heavily degraded cathode materials, half-cells were examined which showed spontaneous cell failure behaviour during battery operation [50]. At the beginning of the galvanostatic measurement, the cell was first cycled in a formation process with a low charging and discharging rate of C/10 for a total of three cycles. A specific discharge capacity of 142 mAh/g could be measured. The cell was then subjected to a lifetime test, operated at a constant charge and discharge rate of C/2. The decrease in specific discharge capacity in the fourth cycle, which was initiated due to the higher current rate, can be clearly seen. The specific discharge capacity drops to a value of 122 mAh/g, which corresponds to 85.9% of the initial capacity. As the galvanostatic measurement continues, it becomes apparent that the specific discharge capacity of the cell decreases more rapidly from the 60th cycle and the cell finally fails in the 93rd cycle. The specific discharge capacity suddenly drops from 95 mAh/g to a value of 0 mAh/g. For the quantitative investigation of the lithium concentration distribution, the half-cell was disassembled, the NMC cathode was washed in DMC and LIBS was performed *post mortem*.

The lithium concentration was averaged in the X direction and in the range $\Delta X=0.3$ mm, starting at an X value of $X_0=4.7$ mm (Figure 5.6). In the Y-direction and in the range from $Y_0=7.5$ mm to $Y_1=11.0$ mm, a measurement range (green marked in Figure 5.6 a) was set to study the lithium concentration outside the detected lithium hot spot observed at location X=4.8 mm and Y=7.2 mm. The NMC thick-layer electrodes were initially charged with a very low C-rate (C/50) so that a sufficiently uniform charge state could be set after complete lithium deintercalation. As expected, a similar lithium inhomogeneity was observed after full discharge. The result suggests that the electrode particles on the electrode surface that are in direct contact with the free electrolyte can be charged and discharged faster and more

homogeneously than those particles that are arranged in the area close to the current collector.

Figure 5.6 ABOUT HERE

Figure 5.7 a shows a range of the lithium concentration distribution for a NMC thick film, which showed spontaneous cell failure after 93 cycles. Hereby the measurement area was selected according to Figure 5.6 a, outside the detected lithium hot spot. Similar to Park et al. [56], a slow decrease of lithium concentration from the surface down to the current collector was detected. In the model scheme (Figure 5.7 b) it is shown that the limited transport of lithium-ions within the electrode gradually leads to inhomogeneous reactions. The upper electrode regions are more affected during electrochemical cycling, suggesting that the ohmic loss and concentration polarization in the electrode are increasing. Accompanying side reactions and repeated charging and discharging of the electrode lead to a further increase in the impedance values against the transport of lithium-ions in the electrode. The result is an effectively higher current density in the top layer (Figure 5.7 a, b), which means that the active particles exposed to a higher current density are more susceptible to electrochemical degradation. According to Park et al. [56] cracking is initiated within the particles, followed by SEI reformation at the exposed surfaces. The cracking and resulting surface products increase the complexity of the lithium-ion diffusion pathways, along with the increase in tortuosity. Overall, the proportion of active material that is still available for the electrochemical reactions is reduced. Finally, a considerable amount of the active material in the area close to the current collector can no longer participate in the electrochemical reaction at all. On the other hand, the particles in the top layer of the electrode are exposed to a higher effective current density, with the risk of permanent damage over several cycles.

However, as shown in [50], the lithium mapping of an electrode surface shows in general strong deviations from a homogenous behaviour. The local state of charge in general varies influenced by defects, electrode, and separator inhomogeneities, and external pressure variations on the cell. In case of separator inhomogeneities and their impact on lithium plating this was entirely discussed by Liu et al. [57]. They found that external stresses lead to a local change in separator porosities which in turn induce a variation of current density and thus a local change in state-of-charge or even lithium plating can be detected. A variation in porosity on macro-scale is enforcing the formation of lithium hot spots during electrochemical cycling as shown in [50]. However, also for a homogenous porosity cells show after cell failure the formation of lithium hot spots at cathode side. The cross-sectional depth profile Figure 5.8 a shows clearly that a local increase in lithium concentration is penetrating through all layers down to the current collector. It is worth mentioning, that a local increase in lithium concentration is also observed in an area close to the current collector. Possible reasons for this may indicate insufficient wetting with liquid electrolyte in deeper areas of the electrode where dry areas provide starting points for cell degradation during cycling. However, an uneven pressure distribution during cell assembly could also lead to increased lithium enrichment.

The zones of characteristic lithium concentration profiles are denoted by the "I" to "IV" in Figure 5.8 a. The lithium concentration significantly increases for layers 14 to 26 and especially close to the current collector. The lithium concentration is also most pronounced in the range $Y_{00}(I)=4.5$ mm to $Y_1(I)=5.5$ mm. In layers 2 to 14 the lithium concentration is quite inhomogeneous. The intercalation and deintercalation rate of lithium-ions is reduced in electrode areas close to the current conductor due to the lithium-ion concentration gradient

along the thickness of the electrode layer and a correlated increased diffusion overvoltage. In addition, dry areas of the electrode can accelerate cell degradation. For $Y_0(II)=7.0$ mm to $Y_1(II)=7.4$ mm (marked with "II" in Figure 5.8 a), the lithium concentration in NMC reaches a value of 1.30 at the electrode surface and 1.24 close to the current collector (layer 26). This increase in lithium concentration is an indication that the starting point of degradation started exactly at this electrode position. It can be concluded that the cell failure was initiated due to the lithium concentration profile shown in area "II". For area "III" ($Y_0(III)=7.5$ mm to $Y_1(III)=11.0$ mm), the lithium concentration profile corresponds to the model described by Park et al. [56]: While the upper layer particles are exposed to higher current densities, the lower region of the electrode remains largely inactive during electrochemical cycling. The increased lithium concentration is due to cracking or formation of reaction products during the cycling process. The marked area "IV" is equivalent to area "I", whereby the increased lithium concentration can already be observed starting from the fourth layer. It is worth mentioning that lithium concentration gradients were observed in both directions. On the one hand, an increased lithium concentration spread from the electrode surface in the direction to the current conductor (area "II") was detected, on the other hand, an increased lithium concentration profile was detected in deeper regions of the composite layer (area "IV" and "I").

<div align="center">Figure 5.8 ABOUT HERE</div>

5.5 3D battery concept and its impact on high-rate capability

The 3D battery concept for ultra-thick film nickel rich NMC cathode materials could be recently established. NMC 622 electrodes with a thickness of up to $250\,\mu m$ and a mass loading of $52\,mg/cm^2$ were realized for this purpose. Structuring using ultrafast laser ablation enables a high aspect ratio and defect free pattern down to the current collector

(Figure 5.9 a). The active mass loss could be reduced to less than 5%. The periodicity of the line pattern is typically in the range of $200\,\mu m$ to $600\,\mu m$ [22]. NMC 622 cathodes were assembled in half cells versus metallic lithium using the coin cell design. The impact of electrode thickness and laser structuring on the rate capability was investigated. Figure 5.9 b shows that for laser-structured NMC 622 electrodes with a thickness of up to $210\,\mu m$, the discharge capacity could be maintained even for high power operation (C-rate of 2C). For cells with unstructured NMC 622 electrodes of same thickness the capacity drops dramatically even for low power operation. An increase in NMC film thickness from state-of-the-art $50\,\mu m$ up to $210\,\mu m$ corresponds to an increase in energy density of about 26 % according to [6]. Thus, it could be proven for the first time for this type of battery system that high energy and high-power operation are possible at the same time.

Figure 5.9 ABOUT HERE

In recent research the 3D battery concept was successfully transferred to next generation electrode materials such as silicon/graphite anodes and NMC 811 cathode materials by introducing line and grid patterns, respectively [28,30,44]. The results of 3D batteries based on thick-film NMC 811 electrodes with a thickness of $100\,\mu m$ show a huge impact with regard to high rate capability for structured electrodes as shown in Figure 5.10 a. It is quite obvious that in the presented case the high rate capability is most efficient for a C-rate of 2C. The respective Nyquist plots (Figure 5.10 b) which were taken prior to the galvanostatic measurements reveal that the charge transfer resistance is smaller for the 3D battery in comparison to the conventional 2D approach. In addition a higher diffusion coefficient was measured for the 3D approach proving the improvement of lithium-ion diffusion kinetics resulting in the increased high rate capability (Figure 5.10 a). For more details refer to [28].

There are several groups worldwide pushing the 3D battery concept towards application level. Currently, most of those research is focused on hole, line, and grid patterns [6,44,58-62]. Numerical studies of electrochemical processes prove that in a first approximation the type of pattern does not matter [63]. The experimental evaluation of lithium concentration profiles in electrodes via LIBS is a suitable approach to support finding appropriate structure design rules (see next sections). However, with regard to wetting of electrode with liquid electrolyte and volume changes during lithiation/delithiation of the active materials, it is expected that free standing structures and capillary features will be very beneficial with regard to battery lifetime. Another aspect to be taken into account for the selected pattern type is the laser process upscaling which might be an issue for selected structure designs.

Figure 5.10 ABOUT HERE

5.6 LIBS analysis on laser-structured model NMC thick-film electrodes

In order to investigate the impact of the 3D battery concept on lithium distribution by LIBS, a model electrode design was selected as described in detail by Smyrek et al. [50]. Free-standing electrode architectures consisting of micro-pillars with geometric dimensions of 600 μm x 600 μm x 100 μm were generated using ultrafast laser ablation, see Figure 5.11.

Figure 5.11 ABOUT HERE

For this type of electrode architecture, due to the laser ablation, in addition to a uniform intrinsic porosity, additional cavity areas (electrolyte reservoirs) were created, which continuously replace the liquid electrolyte consumed during cell cycling. In addition, the porosity value (34% ± 3%) of the free-standing structures corresponds to that of standard NMC 111 thick-film electrodes. In order to be able to evaluate the lithium concentration distribution in free-standing structures and to correlate this together with the electrochemical data with regard to enhanced cell performance, the laser modified NMC cathodes were

assembled into half-cells. Galvanostatic measurements were performed exposing the cells to C-rates of 2C (Figure 5.11). During the formation step, three cycles were performed with a charging and discharging C-rate of C/10. The subsequent C-rate increase was undertaken to study lithium intercalation and its distribution in free-standing architectures under high-current conditions. After a total of 146 cycles, the electrochemical characterization was discontinued so that the electrode could be studied *post mortem* with LIBS after disassembling the cell. During the execution of the LIBS analysis, the NMC micro-pillars generated by means of fs laser radiation were removed very homogeneously down to the current collector.

For laser-structured electrodes, the lithium concentration distribution strongly depends on the charging and discharging current. Figure 5.12 a shows the measured lithium concentration distribution in cross-sectional view of a single micro-pillar of the laser-structured NMC thick-film electrode (see SEM in Figure 5.11) after charging and discharging rate each at C/10 during formation (formation step of Figure 5.11). The shown LIBS lithium mapping was achieved after the respective cell has been completely discharged to a voltage of 3.0 V.

Figure 5.12 ABOUT HERE

During formation at a C-rate of C/10, the long charging and discharging times of each 10 hours ensure a homogeneous intercalation and deintercalation of the lithium-ions as shown in the model scheme in Figure 5.12 b.

At high C-rates of 2C (see Figure 5.11), which corresponds to charging and discharging times of each 30 minutes, the lithium concentration distribution completely changes as reported in [50]. As already postulated by Park et al. [56], the particles which are in direct contact with the free electrolyte guarantee a reduction in cell polarization. It is assumed that

the intercalation/deintercalation of lithium-ions in deeper regions of the electrode - for example close the current collector - mainly takes place via the laser-generated sidewalls in the liquid electrolyte. The tortuosity, i.e., the ratio of the effective lithium-ion diffusion pathway to the theoretically minimum length of pathway (i.e., the electrode film thickness), decreases, leading to an increased effective diffusion coefficient of structured electrodes in comparison to unstructured ones.

It is worth mentioning that the maximum quantitative lithium concentration in the laser generated micro-pillars of the 3D model electrode structured electrodes reaches maximum values of about 1.05 which is only a marginal deviation from the fully-lithiated state of NMC 111. Degradation would be expected for significantly higher lithium concentration values of about 1.3 as illustrated in Figure 5.8. In summary, it can be stated that no degradation processes could be detected for the laser-structured electrodes. However, due to the sensitivity of the LIBS measurement method, it could be clearly shown that new diffusion paths form along the interface between liquid electrolyte and laser-structured side walls, which are activated at elevated C-rates. The change of lithium-ion diffusion pathways and respective lithium concentration profile in micro-pillars as function of C-rate is schematically shown in Figure 5.13. The model scheme is related LIBS studies presented in [50]. The centre of the micro-pillars shows a drop in lithium concentration due to electrochemical cycling at elevated C-rates. In current development this is being compensated by geometric adjustments of the generated structure size.

<div align="center">Figure 5.13 ABOUT HERE</div>

Figure 5.14 shows a comparative study of quantitative lithium concentration profiles in free-standing cathode [50] and anode [43] material because of galvanostatic cycling at elevated C-rates. It can be clearly seen that in both types of electrodes the laser-generated sidewalls

act as new lithium-diffusion pathways. Due to the anisotropy characteristics of flake-like graphite which result in a preferred lithium diffusion parallel to the current collector plane, the impact of laser structuring is even more pronounced. The drop in lithium concentration in the centre of the free-standing structure is more than a factor of two and the penetration depth (half of maximum concentration) indicated by the arrows in Figure 5.14 is about 100 µm and 80 µm for anode and cathode, respectively. This is in good agreement with the experimental results were the most benefit regarding high-rate capability is achieved for structure pitch distances in the order of 200 µm (see Figure 5.9).

Figure 5.14 ABOUT HERE

5.7 Brief summary and perspective for upscaling electrode structuring in production

Structuring of composite electrodes can lead to a doubling of the operational lifetime of the batteries. Furthermore, structuring of anodes boosts the charging performance while structuring of cathodes is required to enable simultaneously high power and high energy battery operation. For realizing high energy batteries, the thick film concept will be flanked with high energy active materials such as nickel rich NMC cathodes, high voltage spinel LMNO cathodes, and silicon-based anodes. However, introducing the 3D battery concept in parallel to the thick film concept significantly improves the electrolyte wetting of the battery materials which finally will lead to a remarkable reduction of scrap rate in battery production. In related research it could be also shown that a positive impact regarding a reduced lithium plating and therefore a benefit with regard to battery safety can be expected as well [64].

Besides an optimization of electrode architectures regarding application scenario, the upscaling of the laser process for integration in battery manufacturing is quite a challenging and rather important task in current research and development. A first approach during

upscaling would be simply increasing the laser power and using ultrashort laser pulses. For thin films and medium size footprints this approach will provide a rather good pattern and surface quality. However, the processing speed has further to be increased as well as the film thickness and electrode footprint for high energy applications. It is worth mentioning, that the process efficiency gets a maximum with regard to the ablation rate per photon if the selected laser energy density is set almost one order of magnitude higher than the removal threshold, which is still a quite small value [6]. Therefore, in terms of ablation efficiency, a further increase in laser power is only meaningful if a multi-beamlet approach is chosen as schematically shown in Figure 5.15. For next generation of ultra-thick film electrodes and large footprint batteries the ultrafast laser structuring process needs to be further optimized regarding its processing speed. A first successful approach was demonstrated by industrial guided projects [42]. A suitable OEM ultrashort pulsed laser radiation source with an average laser power up to 500 W was developed while maintaining the laser pulse duration in the ultrafast regime.

Figure 5.15 ABOUT HERE

The use of ultrafast lasers instead of classical nanosecond lasers is a main precondition to realize laser ablation without any thermal impact to the sensitive active electrode materials. The high average laser power enables the use of a multi-beam laser approach by using diffractive optical elements and a multi-scanner approach (Figure 5.15,). As shown in Figure 5.15, the same laser source can be applied for sub-micron structuring of the current collector by either direct ablation forming so-called LIPSS (laser-induced periodical surface structures) or by direct laser interference processing (DLIP) [65-67]. Laser structuring of current collector foils prior to coating process will gain an enhanced film adhesion which is especially important for silicon-based anodes with huge volume expansion during

electrochemical cycling finally leading to life-extending battery operation. At KIT roll-to-roll infrastructures for laser processing of commercial and sophisticated electrodes with high precision and processing speed are enabling pilot line level. In a first technical approach the processing speed could be increased by a factor of 5. In current national and international projects pouch cells and cylindrical cells with structured electrodes and capacities of 20 Ah and beyond are being built.

References

1. Nishi, Y., *Lithium ion secondary batteries; past 10 years and the future,* Journal of Power Sources, 100(1-2) (2001) 101-106

2. Dühnen, S., Betz, J., Kolek, M., Schmuch, R., Winter, M., Placke, T., *Toward green battery cells: perspective on materials and technologies,* Small Methods, 4(7) (2020) 2000039

3. Partners, H., *Weltweite Preisentwicklung für Lithium-Ionen-Akkus in ausgewählten Jahren von 2010 bis 2019 und eine Prognose bis 2025 (in Euro/kWh),* Statista. Statista GmbH, (2020)

4. Nykvist, B., Nilsson, M., *Rapidly falling costs of battery packs for electric vehicles,* Nature climate change, 5(4) (2015) 329-332

5. Wood III, D.L., Li, J., Daniel, C., *Prospects for reducing the processing cost of lithium ion batteries,* Journal of Power Sources, 275 (2015) 234-242

6. Pfleging, W., *Recent progress in laser texturing of battery materials: a review of tuning electrochemical performances, related material development, and prospects for large-scale manufacturing,* International Journal of Extreme Manufacturing, 3 (2021) 012002 (20pp)

7. Long, J.W., Dunn, B., Rolison, D.R., White, H.S., *Three-dimensional battery architectures,* Chemical Reviews, 104(10) (2004) 4463-4492

8. Smyrek, P., *Laserinduzierte Plasmaspektroskopie an strukturierten Lithium-Nickel-Mangan-Kobalt-Oxid Dickschichtelektroden.* 2022: Karlsruher Institut für Technologie (KIT)

9. Ferrari, S., Loveridge, M., Beattie, S.D., Jahn, M., Dashwood, R.J., Bhagat, R., *Latest advances in the manufacturing of 3D rechargeable lithium microbatteries,* Journal of Power Sources, 286 (2015) 25-46

10. Baggetto, L., Niessen, R.A.H., Roozeboom, F., Notten, P.H.L., *High energy density all-solid-state batteries: A challenging concept towards 3D integration,* Advanced Functional Materials, 18(7) (2008) 1057-1066

11. Xie, J., Oudenhoven, J.F.M., Li, D.J., Chen, C.G., Eichel, R.A., Notten, P.H.L., *High Power and High Capacity 3D-Structured TiO_2 Electrodes for Lithium-Ion Microbatteries,* Journal of the Electrochemical Society, 163(10) (2016) A2385-A2389

12. Kohler, R., Pfleging, W., Proell, J., *Electrode material for lithium-ion batteries and method for its production,* K.I.f. Technology, Editor. 2011: Germany. p. 12

13. Heungsoo, K., Proell, J., Kohler, R., Pfleging, W., Pique, A., *Laser-Printed and Processed LiCoO 2 CathodeThick Films for Li-Ion Microbatteries,* Journal of Laser Micro/Nanoengineering, 7(3) (2012) 320-325

14. Kohler, R., Proell, J., Bruns, M., Ulrich, S., Seifert, H., Pfleging, W., *Conical surface structures on model thin-film electrodes and tape-cast electrode materials for lithium-ion batteries,* Applied Physics A, 112(1) (2013) 77-85

15. Pfleging, W., Kohler, R., Pröll, J., *Laser generated microstructures in tape cast electrodes for rapid electrolyte wetting: new technical approach for cost efficient battery manufacturing,* Proc. of SPIE, 8968 (2014) 89680B-1 - 89680B-8

16. Pröll, J., Kim, H., Mangang, M., Seifert, H.J., Piqué, A., Pfleging, W., *Fs-laser microstructuring of laser-printed $LiMn_2O_4$ electrodes for manufacturing of 3D microbatteries,* Proc. of SPIE, 8968 (2014) 896805-1 - 896805-6

17   Mangang, M., Pröll, J., Tarde, C., Seifert, H.J., Pfleging, W., *Ultrafast laser microstructuring of LiFePO$_4$ cathode material,* Proc. of SPIE, 8968 (2014) 89680M-1 - 89680M-9

18   Pfleging, W., Pröll, J., *A new approach for rapid electrolyte wetting in tape cast electrodes for lithium-ion batteries,* Journal of Materials Chemistry A, 2(36) (2014) 14918-14926

19   Xiong, W., Xia, Q.Y., Xia, H., *Three-dimensional self-supported metal oxides as cathodes for microbatteries,* Functional Materials Letters, 7(5) (2014) 1430003-1 - 1430003-10

20   Mangang, M., *Ultrakurzpulslaserstrukturierung von LiFePO$_4$- und LiMn$_2$O$_4$-Dickschichtelektroden für Lithium-Ionen-Zellen*, in *Fakultät für Maschinenbau, Institut für Angewandte Materialien - Angewandte Werkstoffphysik (IAM-AWP)*. 2019, Karlsruher Institut für Technologie (KIT): Karlsruhe

21   Mangang, M., Seifert, H.J., Pfleging, W., *Influence of laser pulse duration on the electrochemical performance of laser structured LiFePO$_4$ composite electrodes,* Journal of Power Sources, 304 (2016) 24-32

22   Pfleging, W., *A review of laser electrode processing for development and manufacturing of lithium-ion batteries,* Nanophotonics, 7(3) (2018) 549-573

23   Pröll, J., *Lasergestützte Modifikation von Lithiummanganoxid und Lithiumnickelmangankobaltoxid*, in *Fakultät für Maschinenbau, Institut für Angewandte Materialien - Angewandte Werkstoffphysik (IAM-AWP)*. 2014, Karlsruher Institut für Technologie (KIT): Karlsruhe

24   Pröll, J., Kim, H., Piqué, A., Seifert, H.J., Pfleging, W., *Laser-printing and femtosecond-laser structuring of LiMn$_2$O$_4$ composite cathodes for Li-ion microbatteries,* Journal of Power Sources, 255 (2014) 116-124

25   Rakebrandt, J.H., Smyrek, P., Zheng, Y., Seifert, H.J., Pfleging, W., *Laser processing of thick Li(NiMnCo)O$_2$ electrodes for lithium-ion batteries,* Proc. of SPIE, 10092 (2017) 100920M1-100920M7

26   Song, Z.L., Zhu, P.H., Pfleging, W., Sun, J.Y., *Electrochemical performance of thick-film Li(Ni$_{0.6}$Mn$_{0.2}$Co$_{0.2}$)O$_2$ cathode with hierarchic structures and laser ablation,* Nanomaterials, 11(11) (2021) 2962-1 - 2962-16

27   Zhu, P.H., Seifert, H.J., Pfleging, W., *The ultrafast laser ablation of Li(Ni$_{0.6}$Mn$_{0.2}$Co$_{0.2}$)O$_2$ electrodes with high mass loading,* Applied Sciences-Basel, 9(19) (2019) 4067-1 - 4067-15

28   Tran, M.X., Smyrek, P., Park, J., Pfleging, W., Lee, J.K., *Ultrafast-Laser Micro-Structuring of LiNi0. 8Mn0. 1Co0. 1O2 Cathode for High-Rate Capability of Three-Dimensional Li-ion Batteries,* Nanomaterials, 12(21) (2022) 3897

29   Meyer, A., Ball, F., Pfleging, W., *The effect of silicon grade and electrode architecture on the performance of advanced anodes for next generation lithium-ion cells,* Nanomaterials, 11(12) (2021) 3448-1 - 3448-26

30   Zheng, Y., Yin, D., Seifert, H.J., Pfleging, W., *Investigation of Fast-Charging and Degradation Processes in 3D Silicon–Graphite Anodes,* Nanomaterials, 12(1) (2022) 140

31   Zhu, P., Han, J., Pfleging, W., *Characterization and Laser Structuring of Aqueous Processed Li (Ni$_{0.6}$Mn$_{0.2}$Co$_{0.2}$)O$_2$ Thick-Film Cathodes for Lithium-Ion Batteries,* Nanomaterials, 11(7) (2021) 1840

32   Li, Z., Wei, X., Yang, Z., *Pulsed Laser 3D-Micro/Nanostructuring of Materials for Electrochemical Energy Storage and Conversion,* Progress in Materials Science, (2022) 101052

33   Armand, M., Axmann, P., Bresser, D., Copley, M., Edstrom, K., Ekberg, C., et al., *Lithium-ion batteries - current state of the art and anticipated developments,* Journal of Power Sources, 479 (2020) 228708-1 - 228708-26

34   Bortolotti, M., Becker, B., Gil Bardají, M.E., Durand, J.-M., Duarte, M.J., Clerens, P., et al., *European energy storage technology development roadmap towards 2030,* Int. Energy Storage Policy Regul Work, https://ease-storage.eu/wp-content/uploads/2015/10/EASE-EERA-recommendations-Roadmap-LR.pdf, 108 (2017)

35   Kabir, M.M., Demirocak, D.E., *Degradation mechanisms in Li-ion batteries: a state-of-the-art review,* International Journal of Energy Research, 41(14) (2017) 1963-1986

36   Hou, H., Zorba, V., *3D chemical imaging of Li-ion batteries using femtosecond laser plasma spectroscopy,* IEEE Conference on Lasers and Electro-Optics (CLEO) - Laser Science to Photonic Applications, (2014) 1-2

37   Zorba, V., Syzdek, J., Mao, X.L., Russo, R.E., Kostecki, R., *Ultrafast laser induced breakdown spectroscopy of electrode/electrolyte interfaces,* Applied Physics Letters, 100(23) (2012) 234101-1 - 234101-5

38   Imashuku, S., Taguchi, H., Fujieda, S., Suzuki, S., Wagatsuma, K., *Three-dimensional lithium mapping of graphite anode using laser-induced breakdown spectroscopy,* Electrochimica Acta, 293 (2019) 78-83

39   Imashuku, S., Taguchi, H., Kawamata, T., Fujieda, S., Kashiwakura, S., Suzuki, S., et al., *Quantitative lithium mapping of lithium-ion battery cathode using laser-induced breakdown spectroscopy,* Journal of Power Sources, 399 (2018) 186-191

40   Imashuku, S., Taguchi, H., Kawamata, T., Yorifuji, H., Fujieda, S., Kashiwakura, S., et al., *Simpler method for acquiring quantitative state-of-charge distribution of lithium-ion battery cathode with high accuracy,* Journal of the Electrochemical Society, 166(10) (2019) A1972-A1976

41   Park, J., Song, H., Jang, I., Lee, J., Um, J., Bae, S.G., et al., *Three-dimensionalization via control of laser-structuring parameters for high energy and high power lithium-ion battery under various operating conditions,* Journal of Energy Chemistry, 64 (2022) 93-102

42   Meyer, A., Sterzl, Y., Xiao, S., Rädel, U., Pfleging, W., *Ablation behaviour of electrode materials during high power and high repetition rate laser structuring,* Proc. of SPIE, 11989 (2022) 119890G-1

43   Zheng, Y., Pfäffl, L., Seifert, H.J., Pfleging, W., *Lithium distribution in structured graphite anodes investigated by laser-induced breakdown spectroscopy,* Applied Sciences, 9(20) (2019) 4218

44   Zheng, Y., Seifert, H., Shi, H., Zhang, Y., Kübel, C., Pfleging, W., *3D silicon/graphite composite electrodes for high-energy lithium-ion batteries,* Electrochimica Acta, 317 (2019) 502-508

45   Zhu, P., Seifert, H.J., Pfleging, W., *The ultrafast laser ablation of Li $(Ni_{0.6}Mn_{0.2}Co_{0.2})O_2$ electrodes with high mass loading,* Applied Sciences, 9(19) (2019) 4067

46   Song, Z., Zhu, P., Pfleging, W., Sun, J., *Electrochemical performance of thick-film Li (Ni$_{0.6}$Mn$_{0.2}$Co$_{0.2}$)O$_2$ cathode with hierarchic structures and laser ablation,* Nanomaterials, 11(11) (2021) 2962

47   Smyrek, P., Pröll, J., Seifert, H., Pfleging, W., *Laser-induced breakdown spectroscopy of laser-structured Li (NiMnCo) O2 electrodes for lithium-ion batteries,* Journal of the Electrochemical Society, 163(2) (2015) A19

48   Kramida, A., Ralchenko, Y., Reader, J., Team, N.A., *NIST atomic spectra database (version 5.8),* National Institute of Standards and Technology, (2020)

49   Lednev, V.N., Yakovlev, A.V., Labutin, T.A., Popov, A.M., Zorov, N.B., *Selection of an analytical line for determining lithium in aluminum alloys by laser induced breakdown spectrometry,* Journal of Analytical Chemistry, 62(12) (2007) 1151-1155

50   Smyrek, P., Bergfeldt, T., Seifert, H.J., Pfleging, W., *Laser-induced breakdown spectroscopy for the quantitative measurement of lithium concentration profiles in structured and unstructured electrodes,* Journal of Materials Chemistry A, 7(10) (2019) 5656-5665

51   Pfleging, W., Zheng, Y., Mangang, M., Bruns, M., Smyrek, P., *Laser processes and analytics for high power 3D battery materials,* Proc. of SPIE, 9740 (2016) 974013 (9pp)

52   Pfleging, W., Smyrek, P., Hund, J., Bergfeldt, T., Pröll, J. *Surface micro-structuring of intercalation cathode materials for lithium-ion batteries: a study of laser-assisted cone formation.* in *Laser-based Micro-and Nanoprocessing IX.* 2015. International Society for Optics and Photonics

53   Park, J., Jeon, C., Kim, W., Bong, S.J., Jeong, S., Kim, H.J., *Challenges, laser processing and electrochemical characteristics on application of ultra-thick electrode for high-energy lithium-ion battery,* Journal of Power Sources, 482 (2021) 228948-1 - 228948-9

54   Singh, M., Kaiser, J., Hahn, H., *Thick electrodes for high energy lithium ion batteries,* Journal of the Electrochemical Society, 162(7) (2015) A1196-A1201

55   Lee, B.S., Wu, Z.H., Petrova, V., Xing, X., Lim, H.D., Liu, H.D., et al., *Analysis of rate-limiting factors in thick electrodes for electric vehicle applications,* Journal of the Electrochemical Society, 165(3) (2018) A525-A533

56   Park, K.Y., Park, J.W., Seong, W.M., Yoon, K., Hwang, T.H., Ko, K.H., et al., *Understanding capacity fading mechanism of thick electrodes for lithium-ion rechargeable batteries,* Journal of Power Sources, 468 (2020) 228369-1 - 228369-8

57   Liu, X.M., Fang, A., Haataja, M.P., Arnold, C.B., *Size dependence of transport non-uniformities on localized plating in lithium-ion batteries,* Journal of The Electrochemical Society, 165(5) (2018) A1147

58   Matsumoto, F., Yamada, M., Tsuta, M., Nakamura, S., Ando, N., Soma, N., *Review of the structure and performance of through-holed anodes and cathodes prepared with a picosecond pulsed laser for lithium-ion batteries,* International Journal of Extreme Manufacturing, (2022)

59   Kriegler, J., Hille, L., Stock, S., Kraft, L., Hagemeister, J., Habedank, J.B., et al., *Enhanced performance and lifetime of lithium-ion batteries by laser structuring of graphite anodes,* Applied Energy, 303 (2021) 117693

60   Chen, K.-H., Namkoong, M.J., Goel, V., Yang, C., Kazemiabnavi, S., Mortuza, S., et al., *Efficient fast-charging of lithium-ion batteries enabled by laser-patterned three-*

dimensional graphite anode architectures, Journal of Power Sources, 471 (2020) 228475

61   Dunlap, N., Sulas-Kern, D.B., Weddle, P.J., Usseglio-Viretta, F., Walker, P., Todd, P., et al., *Laser ablation of Li-ion electrodes for fast charging: Material properties, rate capability, Li plating, and wetting,* Journal of Power Sources, 537 (2022) 231464

62   Park, J., Hyeon, S., Jeong, S., Kim, H.-J., *Performance enhancement of Li-ion battery by laser structuring of thick electrode with low porosity,* Journal of Industrial and Engineering Chemistry, 70 (2019) 178-185

63   Schweighofer, L., Eschelmüller, B., Fröhlich, K., Pfleging, W., Pichler, F., *Modelling and Optimisation of Laser-Structured Battery Electrodes,* Nanomaterials, 12(9) (2022) 1574

64   Habedank, J.B., Kriegler, J., Zaeh, M.F., *Enhanced fast charging and reduced lithium-plating by laser-structured anodes for lithium-ion batteries,* Journal of The Electrochemical Society, 166(16) (2019) A3940

65   Zheng, Y., An, Z., Smyrek, P., Seifert, H.J., Pfleging, W., Kunze, T., et al. *Laser interference patterning and laser-induced periodic surface structure formation on metallic substrates.* in *2016 IEEE International Conference on Manipulation, Manufacturing and Measurement on the Nanoscale (3M-NANO).* 2016. IEEE

66   Zheng, Y., An, Z., Smyrek, P., Seifert, H., Kunze, T., Lang, V., et al. *Direct laser interference patterning and ultrafast laser-induced micro/nano structuring of current collectors for lithium-ion batteries.* in *Laser-based Micro-and Nanoprocessing X.* 2016. SPIE

67   Zhang, N., Zheng, Y., Trifonova, A., Pfleging, W., *Laser structured Cu foil for high-performance lithium-ion battery anodes,* Journal of Applied Electrochemistry, 47(7) (2017) 829-837
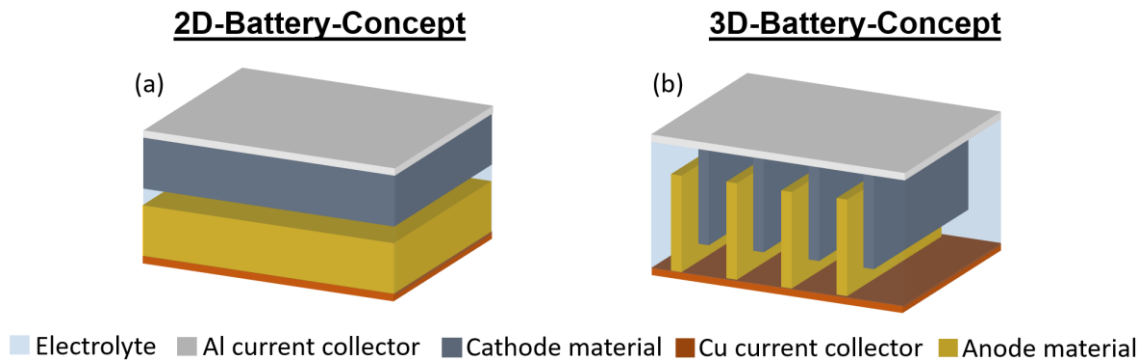
List of figures and figure captions

2D-Battery-Concept (a)

3D-Battery-Concept (b)

Electrolyte   Al current collector   Cathode material   Cu current collector   Anode material

Figure 5.1: Schematic representation of the (a) 2D and (b) 3D battery concept for micro-scaled batteries. Reproduced from [8].

	Energy density	Power density	Fast charging	Cell lifetime
2021 (today)	160 – 260 Wh/kg 450 – 730 Wh/l	340 – 500 W/kg ca. 1000 W/l	15 – 30 min (full electric vehicle, FEV)	≈ 5000 cycles (in combination with C-Anodes)
2030 (in future)	275 – 320 Wh/kg 750 – 900 Wh/l	800 – 1200 W/kg ca. 2000 W/l	10 – 15 min (full electric vehicle, FEV)	≈ 10000 cycles (in combination with C-Anodes)

Figure 5.2: Performance indicators (at cell level) for research and development of lithium-ion batteries extracted from data by Armand et al. [33] and the European Energy Storage Technology Development Roadmap [34].
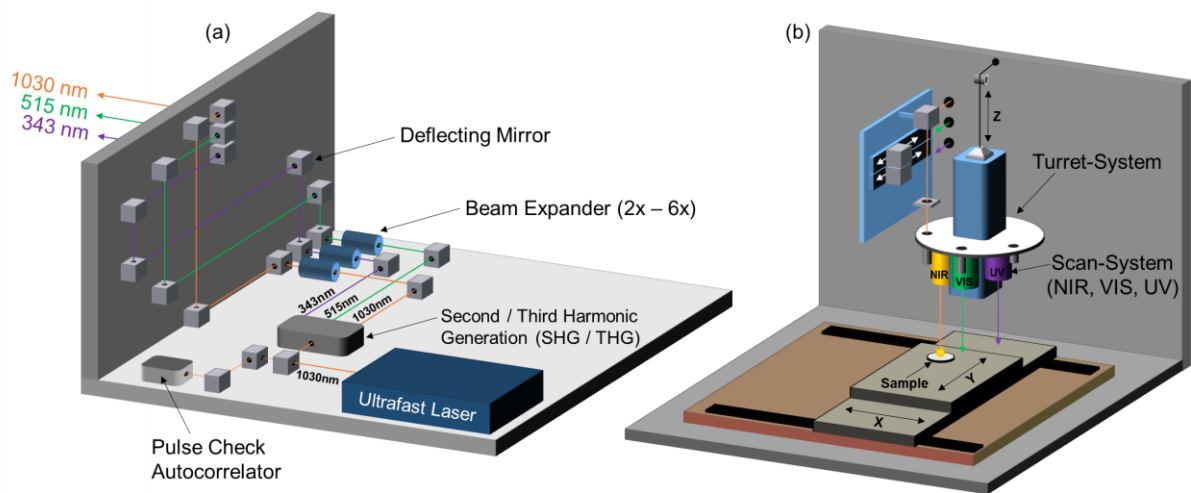
Figure 5.3:   Schematic representation of the PS450-TO type laser processing system: arrangement of (a) the beam path and (b) the laser processing chamber. Reproduced from [8].
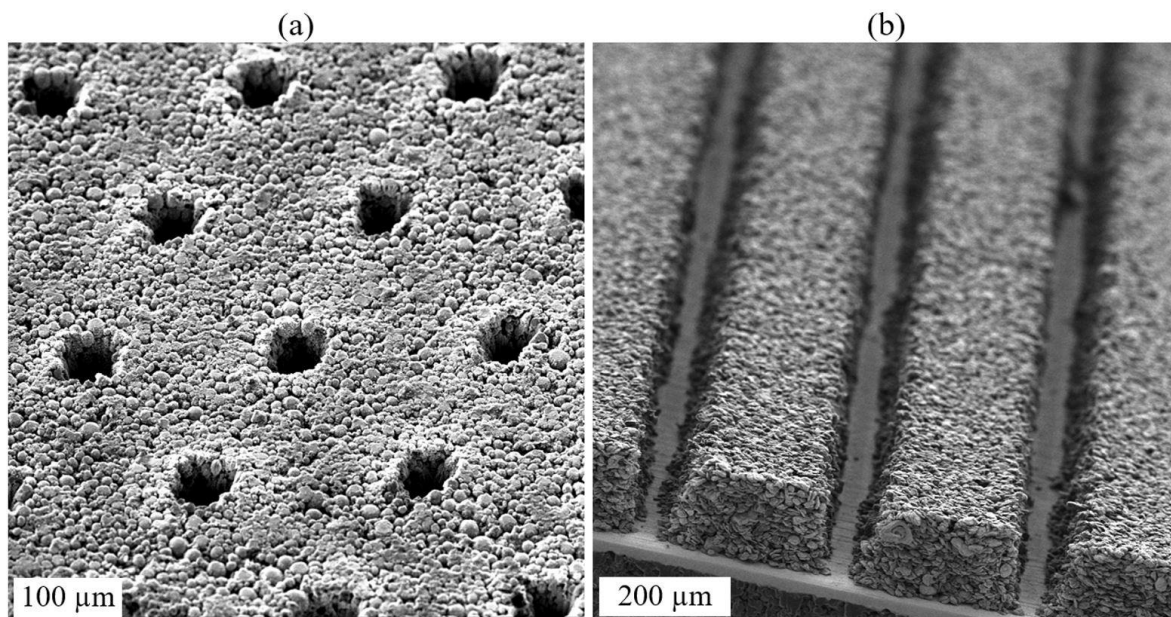
Figure 5.4:   SEM images of ultrafast laser-structured electrodes: (a) Hole pattern in NMC 811 cathode and (b) line pattern in graphite anode.
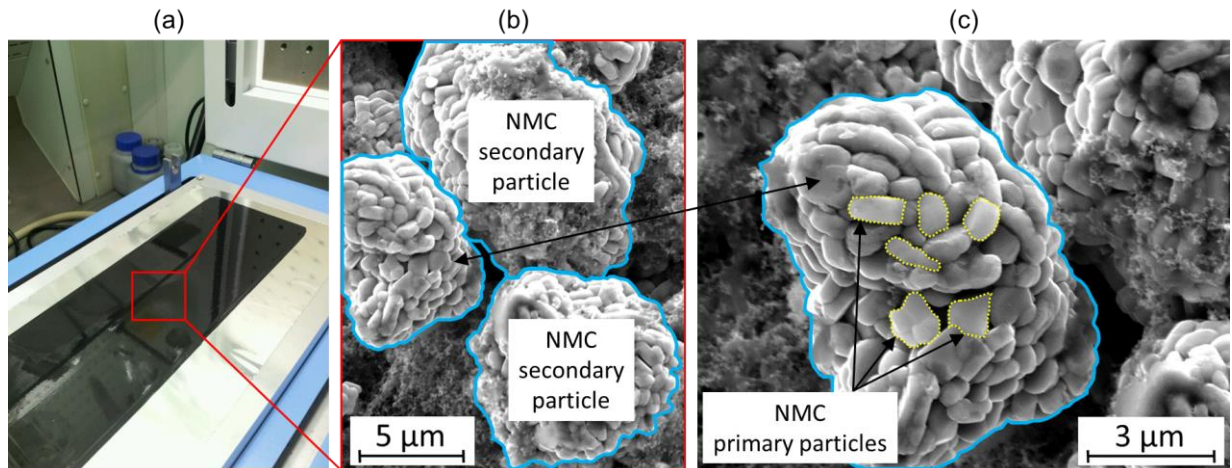
Figure 5.5: Fabrication and characterization of NMC 111 thick film cathodes: (a) Photograph of the electrode thick film (wet film) after the coating process (film casting process), (b) SEM image of the surface of an NMC thick film cathode after the drying process. The blue-framed particles identify the NMC secondary particles, which consist of primary particles - shown in (c) with yellow dashed lines. Reproduced from [8].
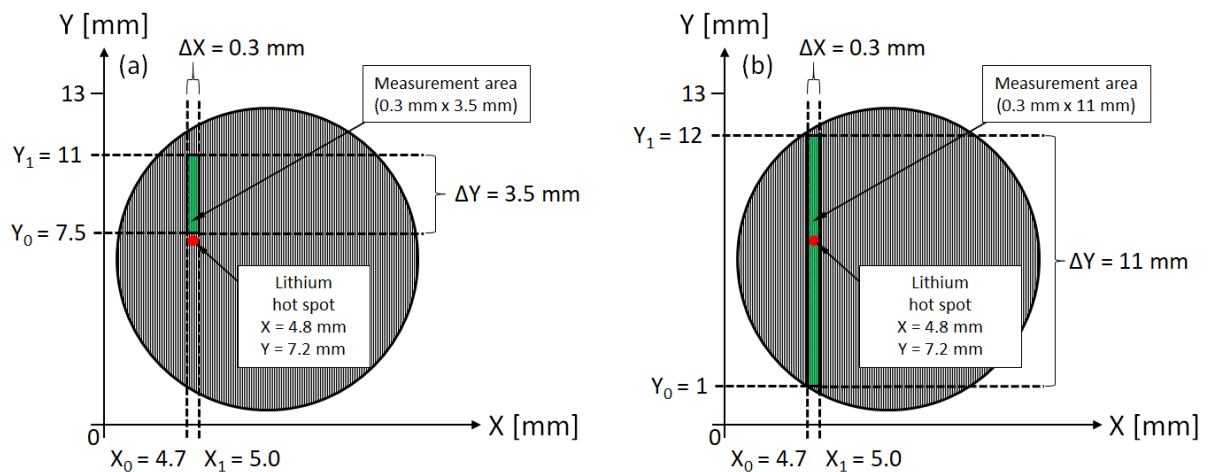
Figure 5.6: LIBS measurement ranges (marked in green) for investigating the lithium concentration distribution in unstructured and degraded NMC thick-film electrodes: (a) measurement range outside a detected lithium hot spot at (X=4.8 mm and Y=7.2 mm). (b) Measurement range covering the lithium hot spot. Reproduced from [8].

(a)

x in $Li_x(Ni_{1/3}Mn_{1/3}Co_{1/3})O_2$

lower lithium concentration close to current collector regions

(b)

Lithium concentration
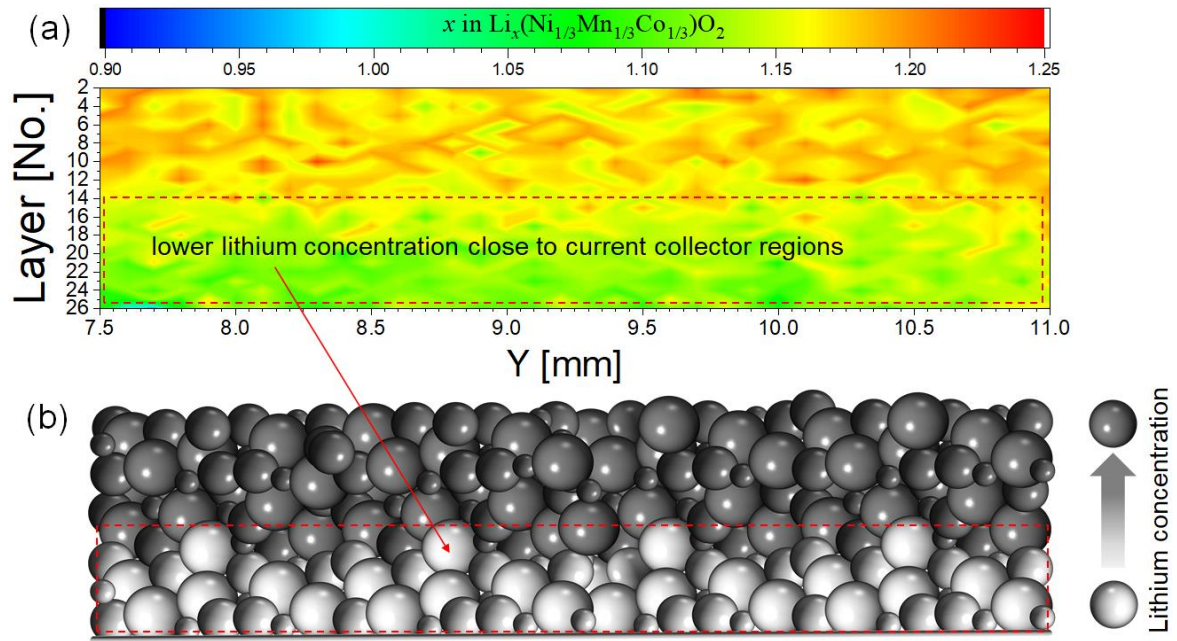
Figure 5.7: LIBS analysis (depth profile in cross sectional view) of a NMC 111 thick film cathode (measurement range shown in Figure 5.6 a): (a) X-direction averaged lithium concentration profile (quantitative) as a function of the Y-coordinate. (b) Model scheme of the lithium concentration distribution in the discharged state of the cell. Reproduced from [8].
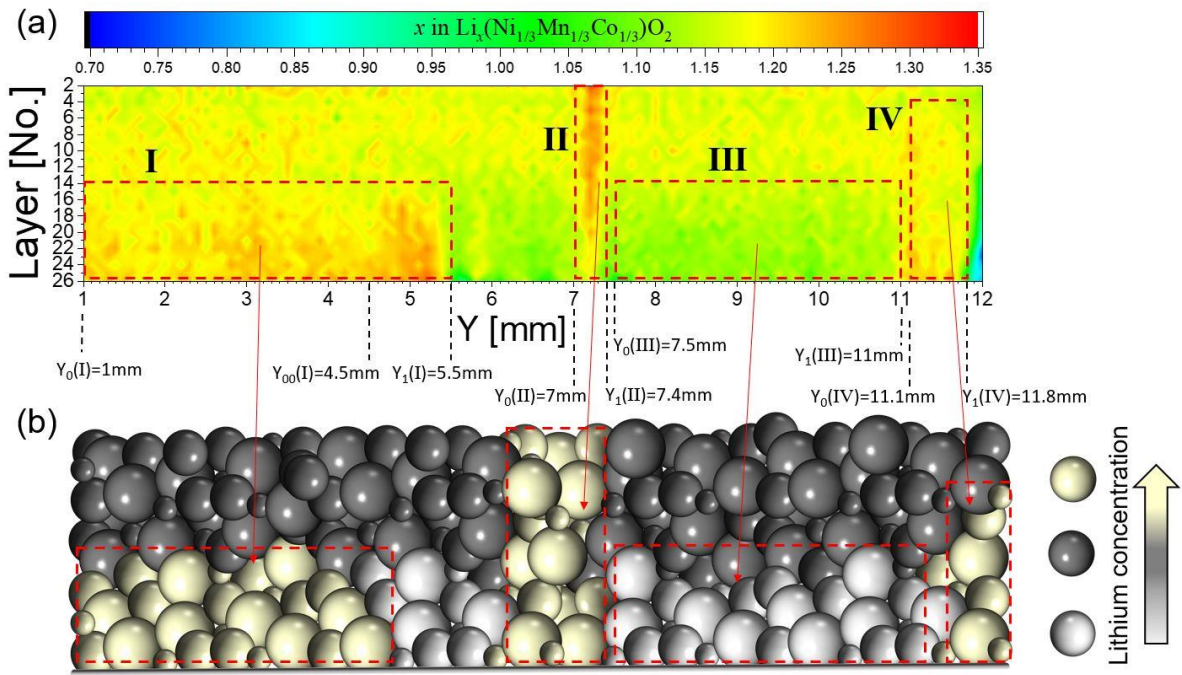
Figure 5.8: *Post mortem* LIBS investigation of unstructured NMC 111 thick-film electrode after spontaneous cell failing described in [50]: (a) 2D lithium distribution in cross sectional view (measurement range shown in Figure 5.6 b). (b) Model scheme derived from LIBS measurements to describe possible degradation processes. Reproduced from [8].
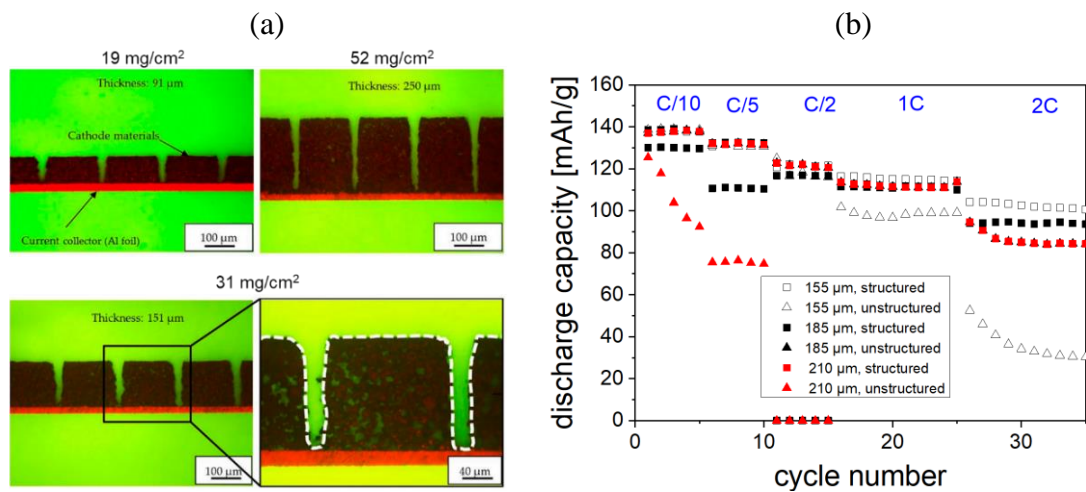
Figure 5.9: Laser structured Li(Ni$_{0.6}$Mn$_{0.2}$Co$_{0.2}$)O$_2$ (NMC 622) cathodes and their impact on electrochemical performance: (a) cross-sectional view of NMC 622 cathodes with different film thicknesses (line distance 200 µm) [45]; (b) specific discharge capacity as

a function of cycle number for lithium-ion cells with structured and unstuctured NMC 111 thick-film electrodes for different discharge C-rates and electrode film thickness (155 µm, 185 µm, 210 µm). Reproduced from [22].

(a)   (b)
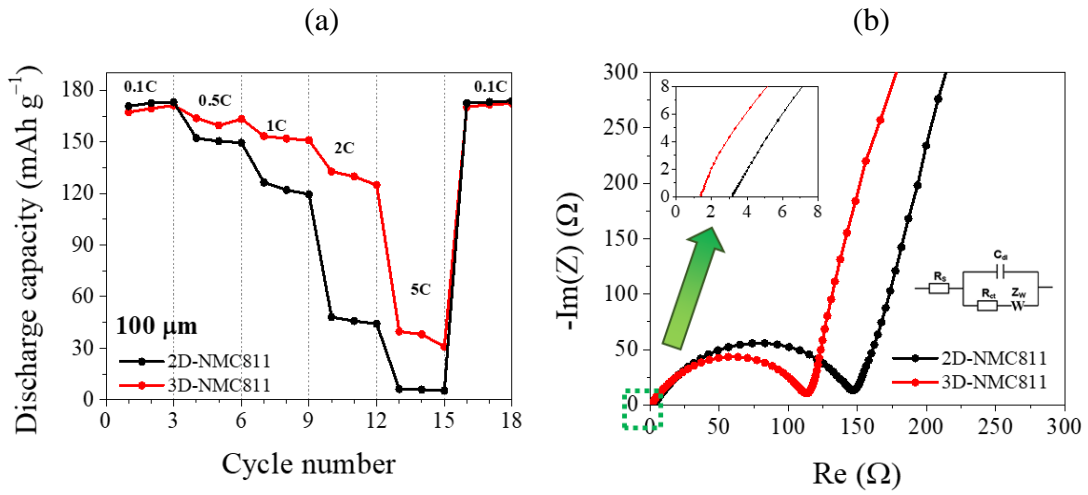
Figure 5.10: Electrochemical performance of cells with laser structured NMC 811 electrodes: (a) Rate capability performance and (b) respective Nyquist plots for unstructured and structured NMC electrodes with thicknesses of 100 µm. Reproduced from [28].
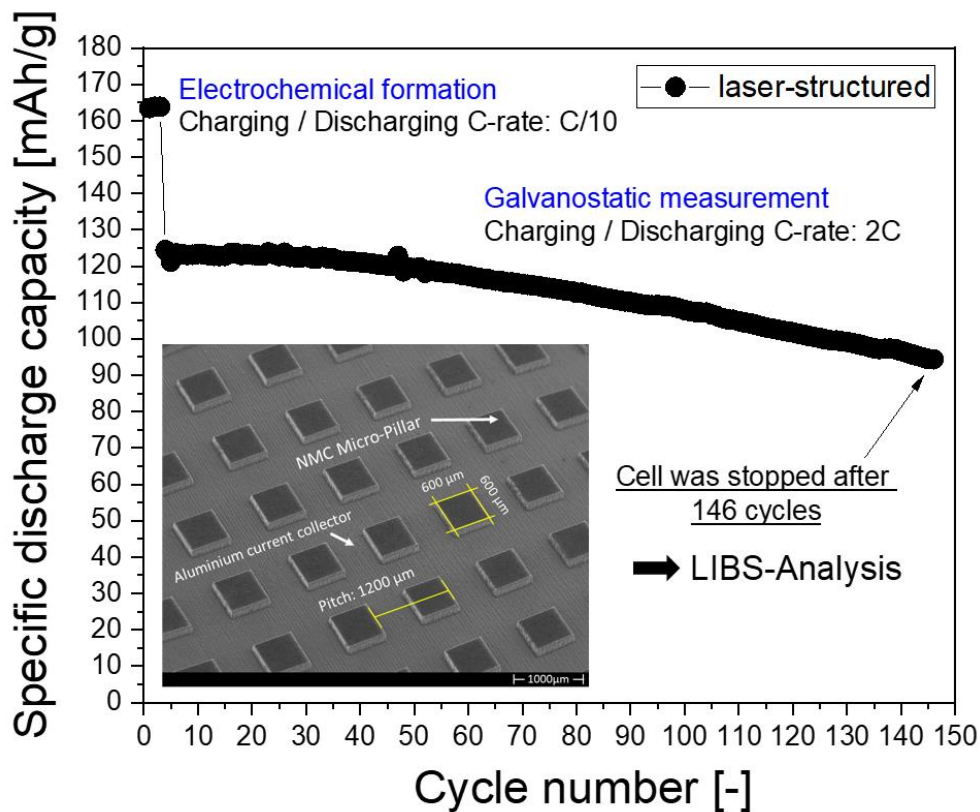
Figure 5.11: Electrochemical characterization of half-cells with laser-structured NMC 111 thick-film model electrode: specific discharge capacity as a function of the number of cycles. The formation was performed with a charge and discharge rate of C/10. From the 4th cycle, the charge and discharge rate was fixed to 2C. After a total number of 146 cycles, cell operation was stopped, the cell disassembled, and the electrode washed out in solvent DMC for subsequent LIBS investigation. The image insert represents an SEM image (top view) of the laser structured NMC thick film at a tilt angle of 30°. For more details refer to [50]. Reproduced from [8].
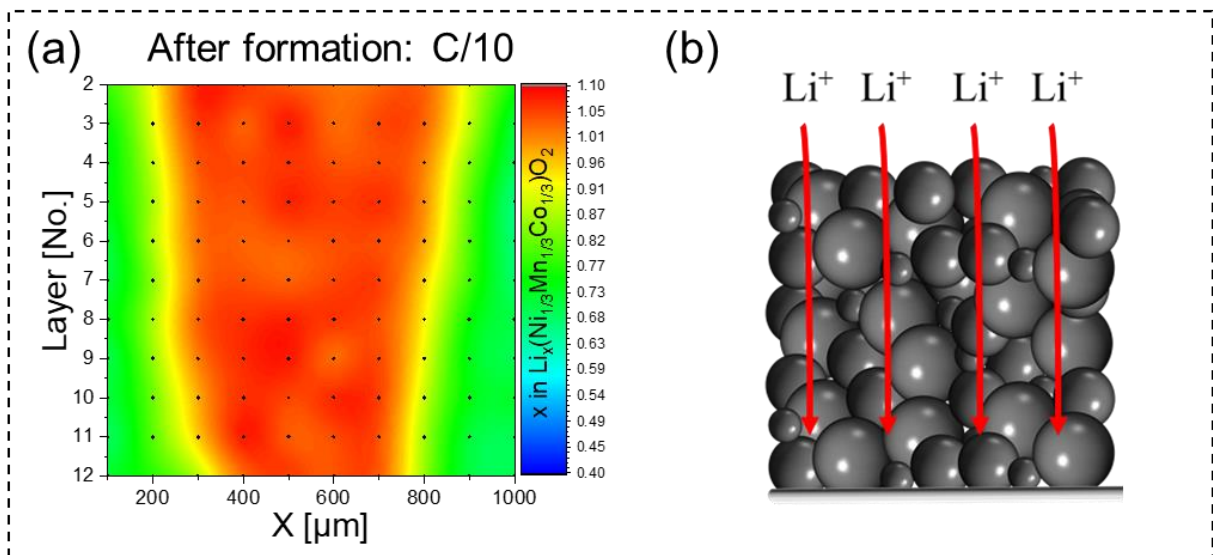
Figure 5.12: Lithium concentration profile in laser-generated NMC electrode (micro-pillar in cross section view) after formation: (a) Measured (*post mortem*) lithium concentration profile after performing the formation step (C-rate of C/10 during charging and discharging) and (b) model scheme of lithium-ion penetration into the micro-pillar. With modifications reproduced from [8].
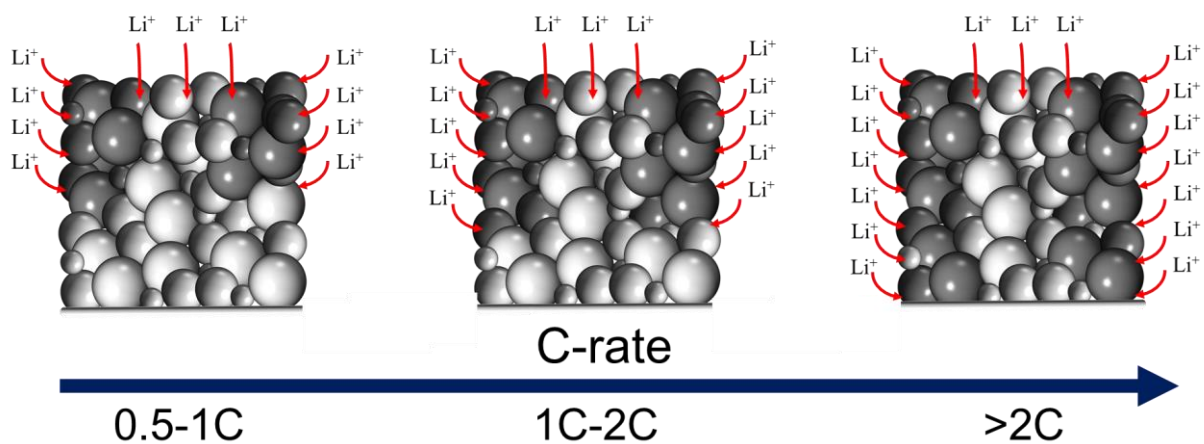

Figure 5.13: Model scheme for lithium diffusion pathways in liquid electrolyte as function of C-rate. The model is referred to model electrode in Figure 5.11.
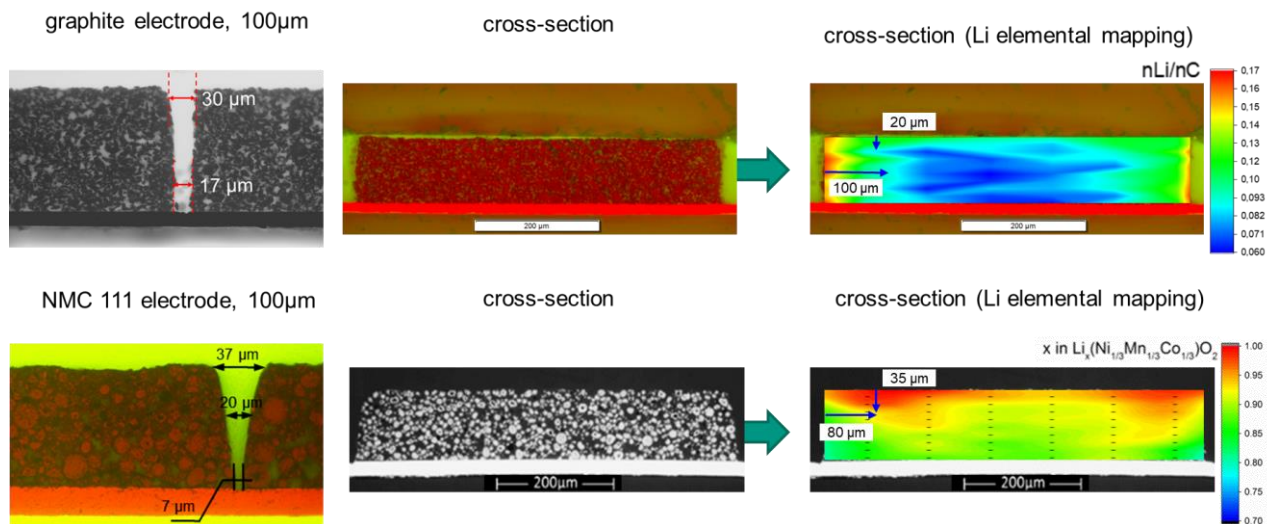
Figure 5.14: Comparative study of lithium concentration profiles in NMC 111 cathode material and flake-like graphite anode material.
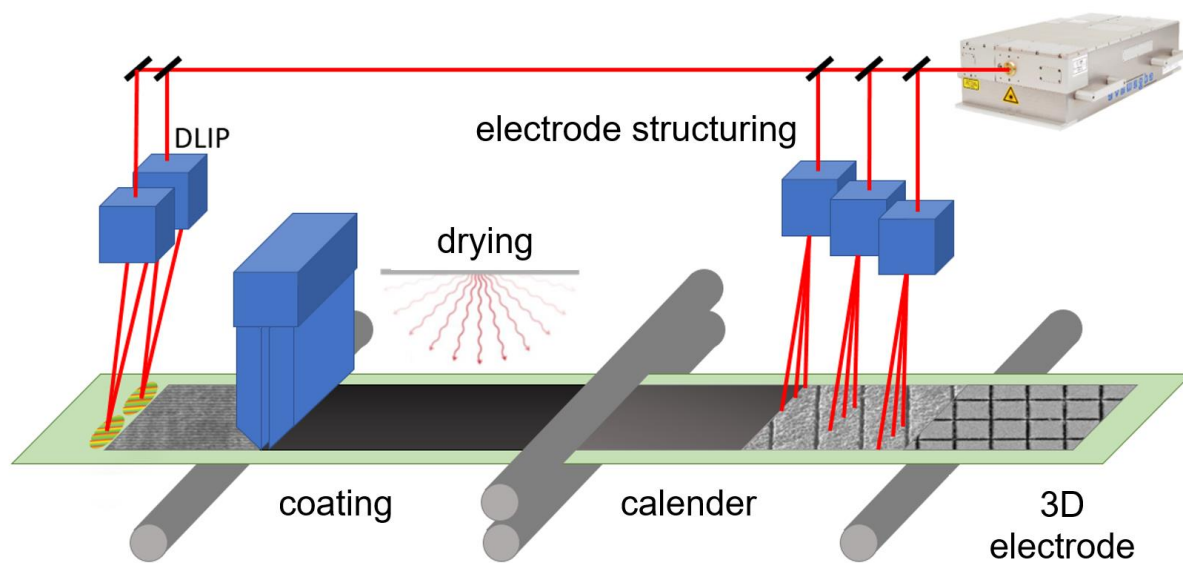

Figure 5.15: Schematic view of a 3D electrode manufacturing process consisting of coating, drying, calendering and a multi-beamlet high power laser approach for high-speed structuring of electrodes and current collectors.